ELECTRON TRANSPORT, PENETRATION DEPTH, AND THE UPPER CRITICAL MAGNETIC FIELD IN ZrB$_{12}$ AND MgB$_2$

V. A. Gasparov[*], **N. S. Sidorov, I. I. Zver'kova, S. S. Khassanov, M. P. Kulakov**

Institute of Solid State Physics, Russian Academy of Sciences
142432, Chernogolovka, Moscow Region, Russia

We report on the synthesis and measurements of the temperature dependences of the resistivity ρ, the penetration depth λ, and the upper critical magnetic field H_{c2} for polycrystalline samples of dodecaboride ZrB$_{12}$ and diboride MgB$_2$. We conclude that ZrB$_{12}$ behaves as a simple metal in the normal state with the usual Bloch–Grüneisen temperature dependence of $\rho(T)$ and with a rather low resistive Debye temperature $T_R = 280$ K (to be compared to $T_R = 900$ K for MgB$_2$). The $\rho(T)$ and $\lambda(T)$ dependences for these samples reveal a superconducting transition in ZrB$_{12}$ at $T_c = 6.0$ K. Although a clear exponential $\lambda(T)$ dependence in MgB$_2$ thin films and ceramic pellets was observed at low temperatures, this dependence was almost linear for ZrB$_{12}$ below $T_c/2$. These features indicate an s-wave pairing state in MgB$_2$, whereas a d-wave pairing state is possible in ZrB$_{12}$. In disagreement with conventional theories, we found a linear temperature dependence of $H_{c2}(T)$ for ZrB$_{12}$ ($H_{c2}(0) = 0.15$ T).

PACS: 74.70.Ad, 74.25.Op, 72.15.Gd

1. INTRODUCTION

The recent discovery of superconductivity at 39 K in magnesium diboride [1] has initiated a booming activity in condensed matter physics. This activity has raised considerable interest in the search for superconductivity in other borides [2]. Unfortunately, none of natural candidate MeB$_2$-type diborides of light metals (Me = Li, Be, Al, Ca) nor any of a large number of the known isostructural transition metal diborides (Me = = Ti, Zr, Hf, V, Ta, Cr, Mo, U) have been found to be superconducting [2]. Superconductivity was observed [3–6] only in nonstoichiometric compounds (MoB$_{2.5}$, NbB$_{2.5}$, Mo$_2$B, W$_2$B, BeB$_{2.75}$). We note that the earlier speculation about superconductivity in TaB$_2$ [7] (in contradiction to other published data [2]) has been disproved by recent resistivity, susceptibility, and specific heat measurements supported by electronic structure calculations [8].

These results do not seem to support the application of the old idea about superconductivity in metallic hydrogen [9] to the explanation of superconductivity in MgB$_2$ [10]. In spite of this fact, we discuss some aspects of this idea. In particular, it is believed that in MgB$_2$, the averaged phonon frequencies (in other words, the Debye temperature) must be very high due to the low mass of the boron, which sharply increases the prefactor in the McMillan formula for T_c. Indeed, the band structure calculations have shown that electrons at the Fermi level are predominantly boron-like in MgB$_2$ and the superconductivity is due to graphite-type "metallic" boron sheets [10]. Furthermore, Eremets et al. [11] recently observed that the semiconducting polycrystalline boron (rombohedral β-B$_{105}$) transforms to a metal under high pressure and even to a superconductor at about 160 GPa. The critical temperature T_c increases from 6 K to 11.2 K at raised pressure up to 250 GPa. This observation supports the old idea that a route for optimizing T_c is in preparation of boron-rich compounds, even though this does not yet work for known borides.

In fact, the search for superconductivity in borides has a long history. Matthias et al. [12] discovered several superconducting cubic hexa- and dodecaborides (MeB$_6$ and MeB$_{12}$) in the 1960's. Many other hexa- and dodecaborides (Me = Ce, Pr, Nd, Eu, Gd, Tb, Dy, Ho, Er, Tm) were found to be ferromagnetic or antiferromagnetic. It was suggested that the superconduc-

tivity in YB_6 and ZrB_{12} (having the highest T_c values 6.5–7.1 K and 6.03 K, respectively [3]) might be due to the hypothetical cubic metallic boron. However, a much smaller isotope effect on T_c for boron in comparison with the Zr isotopic substitution suggests that the boron in ZrB_{12} serves as an inert background, and Zr is actually crucial for superconductivity [13, 14], even though chemically, ZrB_{12} mainly contains boron.

While the superconductivity in ZrB_{12} was discovered a long time ago [12], there has been little effort devoted to the study of basic superconductive properties of this dodecaboride. Only recently were the electron transport of solid solutions $Zr_{1-x}Sc_xB_{12}$ [15] and the band structure calculations for ZrB_{12} [16] reported. Understanding the electron transport properties of the cluster borides and the superconductivity mechanism in these compounds is very important. In this paper, we attempt to address this problem. We report the temperature-dependent resistivity $\rho(T)$, magnetic field penetration depth $\lambda(T)$, and upper critical magnetic field $H_{c2}(T)$ for polycrystalline samples of ZrB_{12}. Comparative data on $\rho(T)$ and $\lambda(T)$ in MgB_2 thin films and pellets are also presented.

The structure of this paper is as follows. In Sec. 2, we report on synthesis of ZrB_{12} and MgB_2 and the experimental techniques. Section 3 describes the electron transport in these compounds. Section 4 describes the temperature dependence of λ in thin films and polycrystalline samples. The data on $H_{c2}(T)$ are presented in Sec. 5.

2. EXPERIMENTAL

Under ambient conditions, dodecaboride ZrB_{12} crystallizes in the fcc structure (Fig. 1) of the UB_{12} type (space group $Fm\bar{3}m$), with the lattice parameter $a = 0.74075$ nm [17]. In this structure, the Zr atoms are located at interstitial openings in close-packed B_{12} clusters [15]. In contrast, the diborides show a phase consisting of two-dimensional graphite-like monolayers of boron atoms with a honeycomb lattice, intercalated with metal monolayers [2]. In our search for the superconducting diboride compounds, we observed superconductivity at 5.5 K in ZrB_2 polycrystalline samples that had a few percent amount of ZrB_{12} impurity [2]. It was recently suggested [18] that this observation could be associated with nonstoichiometry in the zirconium sublattice of ZrB_2. To resolve this issue and to study the electron transport and basic superconducting properties of ZrB_{12}, we successfully synthesized this compound.
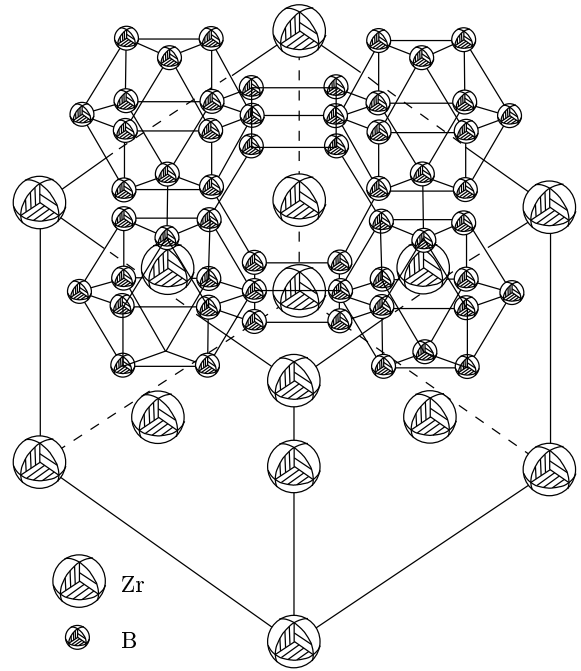

Fig. 1. The lattice structure of dodecaboride ZrB_{12}. For clarity, only B_{12} clusters on the upper face of the lattice are shown

Polycrystalline samples of ZrB_{12} were obtained by the conventional solid-state reaction. The starting materials were a zirconium metal powder (99.99 % purity) and a submicron amorphous boron powder (99.9 % purity). These materials were lightly mixed in appropriate amounts and pressed into pellets 10 mm thick and 20 mm in diameter. The pellets were wrapped in a tungsten foil and baked at 2000 °C by electron-beam heating with subsequent slow cooling to room temperature. The process took place for two hours in a high-vacuum chamber at $2 \cdot 10^{-4}$ Pa. The resulting polycrystalline pellets had over 90 % of the theoretical mass density and were black in color. They demonstrated good metallic conductivity at low temperatures. After regrinding the prepared pellets in an agate mortar, the respective powders were reheated few times for two hours.

The powder X-ray diffraction pattern obtained using CuK_α radiation showed that the samples largely consist of the desired ZrB_{12} phase (Fig. 2). Nevertheless, small amounts of ZrB_2 were found to be present and could not be eliminated by subsequent regrinding and annealing. A Rietveld refinement of the ZrB_{12} X-ray pattern, based on the fcc UB_{12}-type structure presented in Fig. 1, yielded the lattice parameter $a = 0.7388$ nm to be very close to the published val-
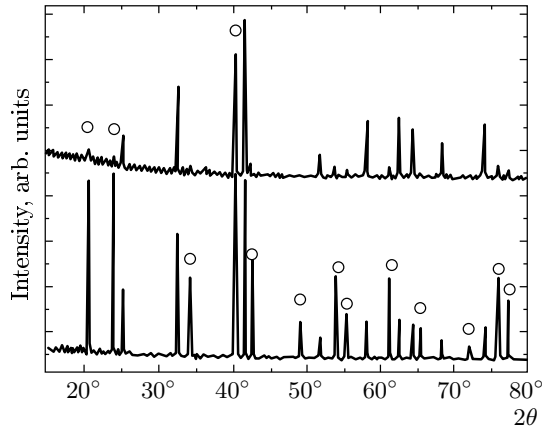
Fig. 2. A typical X-ray $\theta - 2\theta$ scan of ZrB_{12} powders (the lower curve) at room temperature. A similar scan for ZrB_2 pellets studied before [2] is presented by the upper curve. The cycles mark the X-ray reflections from fcc ZrB_{12}

ues [17]. The polycrystalline MgB_2 pellets have been sintered using a similar technique as outlined in our earlier work [2]. This technique is based on the reactive liquid Mg infiltration of boron powder. X-ray diffraction analysis did not reveal the metallic Mg phase, and we therefore believe that a rather high resistivity ratio $(R_{300\ K}/R_{40\ K} = 12)$ is due to the high quality of our samples.

For this study, two highly crystalline, superconducting films of MgB_2 were grown on an r-plane sapphire substrate in a two-step process. Deposition of B precursor films via electron-beam evaporation was followed by *ex-situ* post annealing at $890\,°C$ in the presence of bulk MgB_2 and Mg vapor. Scanning electron microscopy showed dense films with surface roughness below 5 nm. For the measurements, we investigate films of 500 and 700 nm thick, with the corresponding T_c values 38 K and 39 K. The details of the preparation technique are described elsewhere [19].

For the resistance measurements, we used the spark erosion method to cut the pellets into a rectangular bar with dimensions of about $0.5 \times 0.5 \times 8$ mm³. The samples were lapped with a diamond paste. To remove any deteriorated surface layers, the samples were etched: ZrB_{12} in hot nitrogen acid and MgB_2 in 2 % HCl plus water-free ethanol. A standard four-probe ac (9 Hz) method was used for resistance measurements. Electrical contacts were made with Epotek H20E silver epoxy. The temperature was measured with platinum (PT-103) and carbon glass (CGR-1-500) sensors. A well-defined geometry of the samples provided for the precise resistivity measurements.

The measurements were performed in the liquid-helium variable-temperature cryostat in the temperature range between 1.1 and 350 K. Magnetic measurements of the resistivity and the penetration depth on the polycrystalline samples were carried out using a superconducting coil in applied fields of up to 6 T. The dc magnetic field was applied in the direction of the current flow. The critical temperature measured by the radiofrequency (RF) susceptibility [2] and $\rho(T)$ was found to be $T_{c0} = 6.0$ K for ZrB_{12} samples and 39.0 K for MgB_2 samples.

The $\lambda(T)$ dependence in thin films was investigated using a single-coil mutual inductance technique. This technique, originally proposed in [20] and improved in [21], takes advantage of the well-known two-coil geometry. It was successfully used for the observation of the Berezinskii−Kosterlitz−Thouless vortex–antivortex unbinding transition in ultrathin $YBa_2Cu_3O_{7-x}$ films [22] as well as for the study of the $\lambda(T)$ dependence for MgB_2 films [23]. In particular, this RF technique measures the change of inductance ΔL of a one-layer pancake coil located in the proximity of the sample. The coil is a part of the LC circuit driven by a marginal oscillator operating at 2–10 MHz or by the impedance meter (VM-508 TESLA 2–50 MHz). The frequency stability of this oscillator is 10 Hz. The film is placed at a small distance (about 0.1 mm) below the coil and is thermally insulated from the coil by a Teflon foil. Both the sample and the coil are in vacuum, but the coil holder is thermally connected with a helium bath, while the sample holder is isolated and may be heated. During the experiment, the coil was kept at 2.5 K, whereas the sample temperature was varied from 2.5 to 100 K. Such a design allows us to eliminate possible effects in temperature changes in L and C on the measurements. The real part of the complex mutual inductance M between the film and the coil can be obtained as

$$\mathrm{Re}\,M(T) = L_0 \left(\frac{f_0^2}{f^2(T)} - 1 \right), \qquad (1)$$

where L_0 and f_0 are the inductance and the resonant frequency of the circuit without the sample. In the London regime, where high-frequency losses are negligible, one can introduce the difference between the temperature-dependent real part of M of the coil with the sample, $\mathrm{Re}\,M(T)$, and that of the coil at T_0, $\mathrm{Re}\,M_0$. This difference is a function of $\lambda(T)$,

$$\Delta\,\mathrm{Re}\,M(T) = \pi\mu_0 \int_0^\infty \frac{M(q)}{1 + 2q\lambda\,\mathrm{cth}(d/\lambda)}\,dq, \qquad (2)$$

where μ_0 is the magnetic permeability of vacuum, $M(q)$ plays the role of the mutual inductance at a given wave number q in the film plane and depends on the distance between the sample and the coil, d is the sample thickness, and μ_0 is a permeability of a free space (additional details can be found in [21]). A change in $\Delta \operatorname{Re} M(T)$ is detected as a change of the resonant frequency $f(T)$ of the oscillating signal. When inserted in Eq. (2), this change yields a temperature-dependent London penetration depth $\lambda(T)$.

Measurements of $\lambda(T)$ for polycrystalline ZrB_{12} and MgB_2 samples were performed with a similar LC technique but using a rectangular solenoid coil into which the sample was placed. The details of this technique are described elsewhere [24]. For such arrangements, changes in the resonant frequency $f(T) = \omega/2\pi$ of the circuit relative to that above T_c, $f(T_c)$, and at the minimal temperature T_1, $f(T_1)$, are directly related to the inductance of the probe coil and, hence, to $\lambda(T)$ by

$$\lambda(T) - \lambda(T_0) = \delta \frac{f^{-2}(T) - f^{-2}(T_1)}{f^{-2}(T_c) - f^{-2}(T_1)}. \qquad (3)$$

Here, $f(T_c)$ and $f(T_1)$ are the respective resonant frequencies at $T > T_c$ and at the minimal temperature T_1 and $\delta = \sqrt{c^2\rho/2\pi\omega}$ is the skin depth above T_c, which was determined from the resistivity $\rho(T)$ measurements.

3. ELECTRON TRANSPORT

Figure 3 shows the temperature dependence of the resistivity for ZrB_{12} and MgB_2 samples. The inset displays the variation of $\rho(T)$ near the superconducting transition with zero resistance at 6.0 K (the width $\Delta T = 0.04$ K) in ZrB_{12} and at 39 K ($\Delta T = 0.7$ K) in MgB_2 samples. The transition is remarkably narrow for ZrB_{12} samples, which is a clear indication of good-quality samples. The transition temperature is consistent with the previously reported values for ZrB_{12} (6.03 K) [12–14] and is comparably larger than that of ZrB_2 samples (5.5 K) [2]. Although ZrB_{12} mostly contains boron, its room-temperature resistivity is only four times larger than that of MgB_2 and ZrB_2 [2], while the residual resistivity is ten times larger. The resistivity ratio for ZrB_{12} ($\rho(300\,\text{K})/\rho(6\,\text{K}) \approx 4$) is rather low compared to the single-crystal value 10 [25]. Although an X-ray diffraction analysis revealed small amounts of ZrB_2 (the nonsuperconducting phase [25]), apparently there is no influence of this phase on the $\rho(T)$ dependence, because below T_c, the resistivity drops to zero, rather than to the residual value.
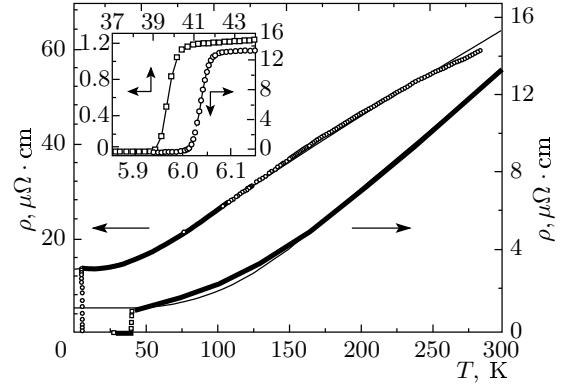

Fig. 3. Temperature dependence of the resistivity ρ for ZrB_{12} (open circles) and MgB_2 (squares) polycrystalline samples. The solid lines represent the Bloch–Grüneisen fits to the experimental data in accordance with Eq. (4)

One can predict a nearly isotropic resistivity for fcc ZrB_{12}, which can be described by the Bloch–Grüneisen (BG) expression of the electron–phonon (e–p) scattering rate [26]:

$$\rho(t) - \rho(0) = 4\rho_1 t^5 \int_0^{1/t} \frac{x^5 e^x dx}{(e^x - 1)^2} = 4\rho_1 t^5 J_5(1/t). \quad (4)$$

Here, $\rho(0)$ is the residual resistivity, $\rho_1 = d\rho(T)/dt$ is the slope of $\rho(T)$ at high temperatures ($T > T_R$), $t = T/T_R$, and T_R is the resistive Debye temperature. As we can see from Fig. 3, the BG equation describes our data reasonably well, indicating the importance of the e–p interaction for both metals. The best fit to our data is obtained with $T_R = 280$ K for ZrB_{12} and $T_R = 900$ K for MgB_2.

In contrast to ZrB_{12}, the resistivity of MgB_2 samples does deviate from the BG model at low temperatures. This problem has been under consideration by several groups. In particular, Putti et al. [27] modified the BG equation by introducing a variable power n for the $t^n J_n(1/t)$ term in Eq. (4). The best fit to the data was obtained with $n = 3$, which in fact ignores a small-angle e–p scattering. Recently, Sologubenko et al. [28] reported a cubic T-dependence in the a,b-plane resistivity below 130 K in single crystals of MgB_2. This was attributed to the interband e–p scattering in transition metals.

We stress that there are strong objections to this modified BG model: (i) the cubic $\rho(T)$ dependence is a theoretical model for large-angle e–p scattering, and no evidence of it was observed in transition and non-
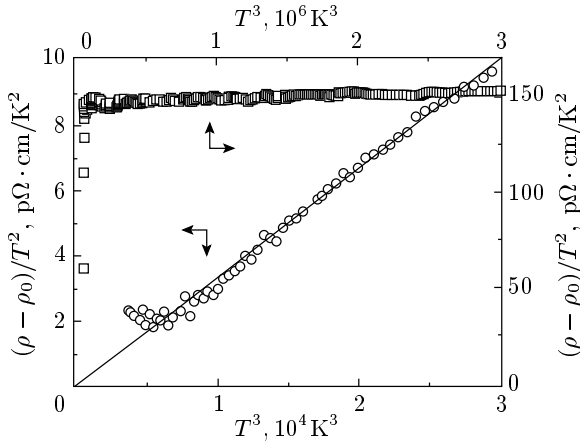
Fig. 4. Temperature dependence of the reduced resistivity $[\rho(T) - \rho(0)]/T^2$ for ZrB_{12} (open circles) and MgB_2 (squares) polycrystalline samples. The solid lines are a guide for the eye

transition metals; (ii) numerous studies of the $\rho(T)$ dependence in transition metals have been successfully described by a sum of the electron–electron (e–e), proportional to T^2, and e–p, proportional to T^5, contributions to the low-temperature resistivity, which may be easily confused with a T^3 law [26, 29, 30]; (iii) the σ–π interband e–p scattering plays no role in normal transport in the two-band model for MgB_2 [31].

To investigate whether a combination of e–e and e–p scattering works for our samples, we decided to add a T^2-term to Eq. (4) [29, 30]. We note that the BG term is proportional to T^5 at low temperatures. Therefore, addition of the T^2-term results in the following expression for the resistivity $\rho(T)$:

$$\frac{\rho(T) - \rho(0)}{T^2} = \alpha + \beta T^3. \qquad (5)$$

Here, α and β are parameters of the respective e–e and e–p scattering terms. When plotted in the $[\rho(T) - \rho(0)]/T^2$ vs T^3 axes, such a dependence yields a straight line with the slope β and the y-intercept ($T = 0$) equal to α. The corresponding plot of our data in Fig. 4 clearly displays the expected linear dependences. The presence of an unusually large T^2-term in MgB_2 data (open squares in Fig. 4) below 150 K is evident ($\alpha = 150$ p$\Omega \cdot$ cm/K^2), whereas the e–p scattering T^5-term is substantially smaller ($\beta = 2.1 \cdot 10^{-6}$ p$\Omega \cdot$ cm/K^5). We note, however, that the α value for MgB_2 is almost 40 times larger than the corresponding values in transition metals such as molybdenum and tungsten ($\alpha_{Mo} = 2.5$ p$\Omega \cdot$ cm/K^2 and

$\alpha_W = 1.5$–4 p$\Omega \cdot$cm/K^2 [29, 30]). In contrast, the ZrB_{12} data display a nearly zero T^2-term.

In general, there are many scattering processes responsible for the T^2-term in the $\rho(T)$ dependence of metals [25]. In particular, umklapp e–e scattering strongly contributes to this term. Furthermore, normal collisions are significant in compensated metals and in thermal resistivity [30]. Borides have a rather high T_R value, which depresses the e–p scattering, and hence the e–e term is easier to observe. Clearly, there is no obvious explanation for such a significant e–e scattering contribution in MgB_2. We believe that additional experiments on purer samples are necessary before the final conclusion about the origin of the T^2-term in the $\rho(T)$ dependence for MgB_2 can be drawn. Besides, the T^2-term was recently observed in ZrB_{12} single-crystal samples with the large resistivity ratio equal to 10 [23]. Apparently, the T^2-term depends on the residual resistivity.

4. PENETRATION DEPTH

Our RF technique allows us to measure the change in the penetration depth $\lambda(T)$ [24]. We note, however, that there is some uncertainty in determining the absolute values of $\lambda(T)$ for bulk samples because of error in the f_0 determination in Eq. (1). For this reason, we do not attempt to determine the absolute values of $\lambda(0)$ for polycrystalline samples from these data but rather find the temperature-dependent part $\Delta\lambda(T) = \lambda(T) - \lambda(1 \text{ K})$. Figure 5 displays the effect of the superconducting transition in ZrB_{12} on $\lambda(T)$. The striking feature of the curves in Fig. 5 is the linear temperature dependence of $\Delta\lambda$ below $T_c/2 = 3$ K. We emphasize that no frequency dependence of these data was found when oscillator frequency was varied by a fact of two.

In the BCS theory, the London penetration depth $\lambda(T, l)$ is identical to the magnetic penetration depth $\lambda(T)$ in the case of specular and diffuse surface scattering and for negligible nonlocal effects, i.e., for $\delta(T, l) \gg \xi(T, l)$ [24, 32]. Here, l is the mean free path of carriers and ξ is the coherence length. In a BCS-type superconductor (with the conventional s-wave pairing) in the clean limit ($l \gg \xi$), the magnetic penetration depth has an exponentially vanishing temperature dependence below $T_c/2$ (where $\Delta(T)$ is almost constant) [32]:

$$\lambda(T) = \lambda(0) \left[1 + \sqrt{\pi \frac{\Delta(0)}{2k_B T}} \exp\left(-\frac{\Delta(0)}{k_B T}\right) \right]. \qquad (6)$$
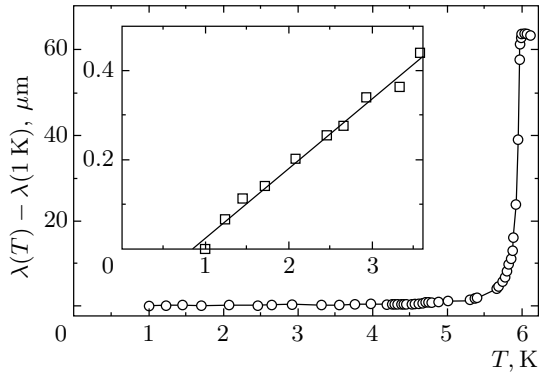
Fig. 5. Temperature dependence of the penetration depth for a ZrB_{12} sample. The solid lines are a guide for the eye. The inset shows the data below 3.5 K in an extended scale

Fig. 6. Temperature variation of the magnetic penetration depth λ for a MgB_2 sample up to T_c. The inset shows the data below $T_c/2$ in an extended scale. The solid line represents the single-gap exponential fit for $\Delta(0) = 2.73$ meV

Here, $\Delta(0)$ is the value of the energy gap and $\lambda(0)$ is the magnetic penetration depth at zero temperature.

At the same time, the unconventional d-wave pairing symmetry causes the energy gap to be suppressed along node lines on the Fermi surface. This results in a linear dependence of $\lambda(T) - \lambda(0) \propto T$ at low temperatures. Such a linear T-dependence of λ was recently used as a fingerprint of the d-wave symmetry for Cooper pairs in cuprate superconductors [33, 34]. From this standpoint, one could argue that the linear $\lambda(T)$ dependence in ZrB_{12} (Fig. 5) may be considered an indication of the d-wave symmetry of the condensate of Cooper pairs.

Recently, however, thermodynamic arguments were suggested [35] that a strictly linear T-dependence of λ at low temperatures violates the third law of thermodynamics, because it produces nonvanishing entropy in the zero-temperature limit. Therefore, one should expect a deviation from the linear T-dependence of λ at very low temperatures. Indeed, recent experiments in cuprates indicate deviation from the linearity of $\lambda(T)$ from the current-carrying zero-energy surface Andreev bound states [36]. We believe that further experiments on single crystals of ZrB_{12} are necessary to confirm the actual character of the $\lambda(T)$ behavior below 1.0 K. Such experiments are now in progress and may shed light on the nature of the pairing state in this dodecaboride.

Figure 6 displays the change in $\lambda(T)$ in a MgB_2 polycrystalline sample. These measurements were done on samples freely placed in a rectangular solenoid coil forming an LC circuit kept at 2.5 K. In Fig. 7, we show the temperature variation of λ for the best MgB_2 film, determined from the one-coil technique and inversion procedure via Eq. (2). A particular feature of these fig-

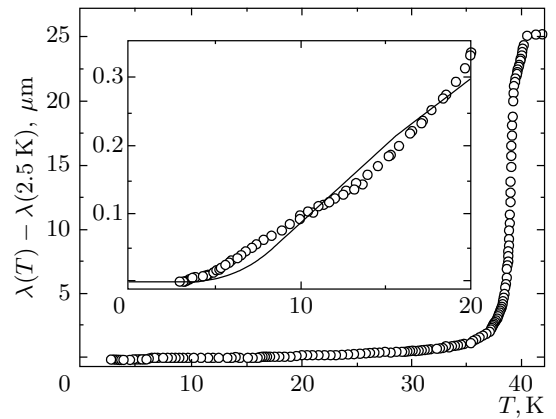**Fig. 7.** Temperature variation of λ up to T_c for a MgB_2 thin film on Al_2O_3. The inset shows the data below $T_c/2$ in an extended scale. The solid line represents the single-gap exponential fit for $\Delta(0) = 2.8$ meV

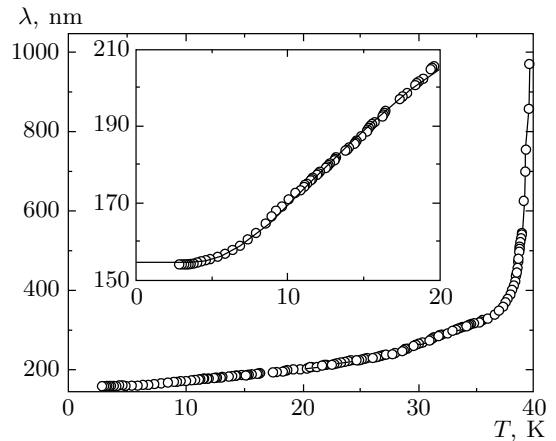ures is a very similar exponential T-dependence at low temperatures for both film and polycrystalline samples. We used the conventional s-wave approach, Eq. (6), to fit these data. In both cases, we observe satisfactory if not perfect agreement between the fits and low-temperature data for thin films. Our fitting parameters (the superconducting gap value at 0 K) are 2.8 and 2.73 meV for film and polycrystalline samples, respectively. The corresponding reduced gap $2\Delta(0)/k_BT_c$ for these samples was found to be 1.64 and 1.62.

Several recent reports on $\lambda(T)$ measurements

[23, 37] in MgB$_2$ provide strong evidence for a predominately exponential temperature dependence of λ at low temperatures, which is consistent with our observation. The reduced gap ontained from exponential fits to the data was found to be 1.42 [37] and 2.3 [23] for single crystals and thin films, respectively. These values, as well as the value we obtained from our data, are significantly smaller than the BCS weak coupling value $2\Delta(0)/k_B T_c = 3.52$. Several other groups have claimed that $\lambda(T)$ in MgB$_2$ does follow a power-law or even linear T-dependence [38]. The possible reason for this discrepancy is that previous studies were limited to temperatures above 4 K, whereas $\lambda(T)$ shows a clear signature of exponential behavior only below 7 K (see Figs. 6 and 7). Another problem may arise in use of nonetched samples, where the damaged surface layer or the proximity effect associated with the presence of a metallic Mg over layer [19] may significantly complicate the use of the surface-sensitive techniques.

We emphasize that our values of the superconducting gap at low temperatures are in the range of values for $3D$ π-bands obtained by point-contact spectroscopy on MgB$_2$ single crystals ($\Delta_\sigma(0) = 7.1$ meV and $\Delta_\pi(0) = 2.9$ meV for the σ- and π-bands, respectively) [39]. Our data also agree with theoretical values predicted by the two-band model [40]. Analysis of the overall temperature dependence of λ within the two-band phenomenological model [41] is now in progress and will be published elsewhere. The essential property of this paper is comparison of the ZrB$_{12}$ and MgB$_2$ low-temperature data, where the $\lambda(T)$ dependence has a totally different behavior.

5. UPPER CRITICAL MAGNETIC FIELD

We now turn to the data on electronic transport in a magnetic field. Figure 8 presents the magnetic-field dependent electric resistivity data for ZrB$_{12}$ polycrystalline samples at various temperatures. Two features are clearly seen: (i) the magnetic field shifts the superconducting transition to lower temperatures; (ii) there is a very small longitudinal magnetoresistivity in the normal state. We extracted the completed upper critical magnetic field H_{c2} by extending the maximal-derivative $d\rho/dH$ line (the dashed line in Fig. 8) up to the normal-state level. The crossing point of this line and the normal-state resistivity gave us the value of H_{c2} at various temperatures as indicated by an arrow in Fig. 8. Despite a clear broadening at higher fields, such onset of the resistive transition remains well defined. We
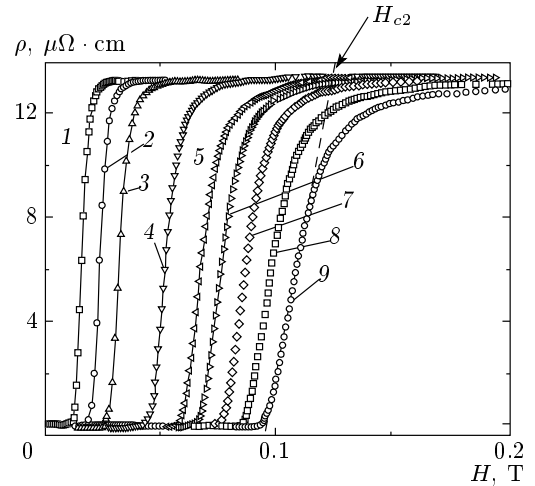

Fig. 8. Magnetic field variation of the resistivity $\rho(T)$ in a linear scale for a ZrB$_{12}$ sample at $T = 5.6$ (*1*), 5.2 (*2*), 5.0 (*3*), 4.3 (*4*), 3.6 (*5*), 3.3 (*6*), 2.0 (*7*), 1.8 (*8*), 1.2 (*9*) K. The solid lines are a guide for the eye and the dashed line describes how the resistive transition field H_{c2} has been established
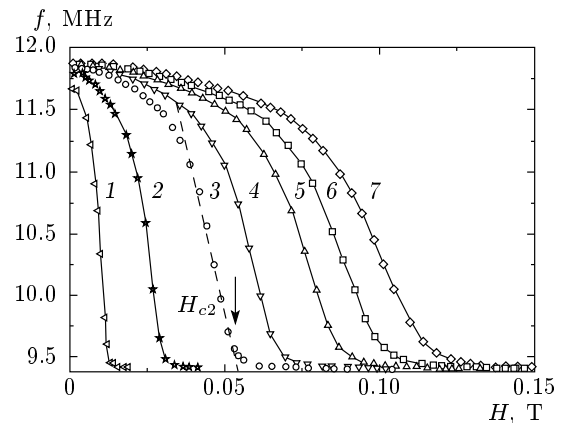

Fig. 9. Magnetic field variation of the resonant frequency of the LC circuit for an ZrB$_{12}$ sample at the temperatures $T = 5.8$ (*1*), 5.0 (*2*), 4.3 (*3*), 3.3 (*4*), 2.3 (*5*), 1.6 (*6*), 1.1 (*7*) K. The solid lines are a guide to the eye and the dashed line describes a linear extrapolation of the RF data used for the $H_{c2}(T)$ determination

note, however, that the resistance may not be an intrinsic property and may be related to the poor grain connection in our polycrystalline samples. Therefore, to obtain a better test for the onset of the superconducting transition, we measured the RF susceptibility.

Figure 9 shows a plot of the temperature dependence of the resonant frequency f of our LC circuit as
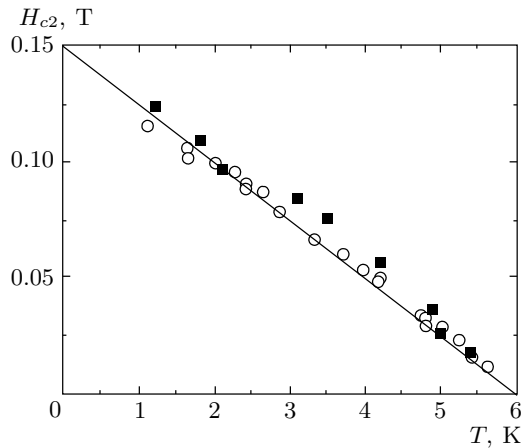
Fig. 10. Temperature variation of the upper critical magnetic field of a ZrB_{12} sample. Different symbols represent the data determined from $\rho(H)$ (squares) and $f(H)$ (circles) data

a function of the longitudinal magnetic field. Changes in the resonant frequency are directly proportional to the RF susceptibility of the sample. To deduce $H_{c2}(T)$, we used a straight-line fit representing the maximum of the derivative df/dH (the dashed line in Fig. 9). This straight line was extended up to the normal-state frequency values. We determined H_{c2} as the crossing point of this line with the normal-state frequency $f_n(T)$. As we can see from Fig. 9, this point is very close to the onset point of $f(T)$ in this plot, which makes determination of $H_{c2}(T)$ more reliable.

Figure 10 presents the $H_{c2}(T)$ data that we deduced from these two techniques. A remarkable feature of this plot is a nearly linear increase of H_{c2} with decreasing temperature for both data with no evidence of saturation down to 1.1 K. To obtain the value of $H_{c2}(0)$ from our RF data, we assumed that

$$H_{c2}(0) = 0.71 T_c \frac{dH_{c2}}{dT}$$

at zero temperature [42]. This assumption yields $H_{c2}(0) = 0.11$ T, which is substantially smaller than the extrapolated value 0.15 T, apparently due to non-BCS or two-gap behavior. Nevertheless, we used this extrapolated number to obtain the coherence length $\xi(0)$ by employing the relation $H_{c2}(0) = \phi_0/2\pi\xi^2(0)$, where ϕ_0 is the magnetic flux quantum. It yields $\xi(0) = 60$ nm, the value which is substantially larger than a few-angstrom coherence length of high-T_c superconductors. The accuracy of our $\lambda(T)$ measurements in ZrB_{12} did not allow us to determine the absolute values of $\lambda(0)$. Therefore, the Ginzburg–Landau parameter

$\kappa = \lambda/\xi$ cannot be determined from these measurements.

Taken as a whole, the temperature dependence of H_{c2} for ZrB_{12} is very similar to that found for MgB_2 [43, 44] and $BaNbO_x$ [45] compounds. Unlike in the conventional BCS theory [42], the $H_{c2}(T)$ dependence is linear over an extended region of temperatures with no evidence of saturation at low temperatures. Although the origin of this feature is not completely understood, similar linear $H_{c2}(T)$ dependences have been observed in other high borides and oxide compounds [43–45].

6. CONCLUSIONS

We successfully performed syntheses of polycrystalline samples of dodecaboride ZrB_{12} and diboride MgB_2. We systematically studied the temperature dependences of the resistivity ρ, the magnetic penetration depth λ, and the upper critical magnetic field H_{c2} in these compounds. The electron transport and superconducting properties have been compared with the aim to shed light on the origin of superconductivity in borides. Although the standard Bloch–Grüneisen expression describes the resistivity data in ZrB_{12} fairly well, a better fit was obtained by adding an electron–electron scattering T^2-term in the $\rho(T)$ dependence of MgB_2. This square term dominates the $\rho(T)$ dependence below 150 K in MgB_2, although is almost zero for ZrB_{12}.

The temperature dependence of λ of both polycrystalline and thin-film MgB_2 samples is well described by an s-wave behavior of the order-parameter symmetry. Our value of the reduced superconducting gap in MgB_2 samples $(2\Delta(0)/k_B T_c = 1.6)$ is significantly smaller than the weak coupling BCS value. However, this value is in a very good agreement with other direct probe measurements of the smaller gap on the π-sheets of the Fermi surface. At the same time, we find that λ in ZrB_{12} has a linear temperature dependence over an extended region of temperatures. This feature may be indicative of the d-wave pairing, although additional measurements are needed for the final conclusion. We find that the upper critical field $H_{c2}(T)$ deduced from RF data is almost the same as that obtained from the resistive data. Both techniques demonstrate an unconventional linear temperature dependence of H_{c2}, with a considerably lower value of $H_{c2}(0) = 0.15$ T. We believe that these observations are clear indicators of the unconventional behavior of electron transport and superconducting properties of dodecaboride ZrB_{12}.

REFERENCES

1. J. Nagamatsu, N. Nakagawa, T. Muranaka et al., Nature **410**, 63 (2001).

2. V. A. Gasparov, N. S. Sidorov, I. I. Zver'kova, and M. P. Kulakov, Pis'ma v Zh. Eksp. Teor. Fiz. **73**, 601 (2001).

3. Z. Fisk, AIP Conf. Proc. № 231 (1991).

4. A. Yamamoto, C. Takao, T. Masui et al., Physica C **383**, 197 (2002).

5. R. Escamilla, O. Lovera, T. Akachi et al., J. Phys.: Condens. Matter **16**, 5979 (2004).

6. D. P. Young, R. G. Goodrich, P. W. Adams et al., Phys. Rev. B **65**, 180518(R) (2002).

7. D. Kaczorowski, A. J. Zaleski, O. J. Zogal, and J. Klamut, E-print archives, cond-mat/0103571; D. Kaczorowski, J. Klamut, and A. J. Zaleski, E-print archives, cond-mat/0104479.

8. H. Rosner, W. E. Pickett, S.-L. Drechsler et al., Phys. Rev. B **64**, 144516 (2001).

9. N. Ashcroft, Phys. Rev. Lett. **21**, 1748 (1968).

10. J. Kortus, I. I. Mazin, K. D. Belashchenko et al., Phys. Rev. Lett. **86**, 4656 (2001).

11. M. L. Eremets, V. V. Struzhkin, H. K. Mao, and R. J. Hemley, Science **203**, 272 (2001).

12. B. T. Matthias, T. H. Geballe, K. Andres et al., Science **159**, 530 (1968).

13. C. W. Chu and H. H. Hill, Science **159**, 1227 (1968).

14. Z. Fisk, A. C. Lawson, B. T. Matthias, and E. Corenzwit, Phys. Lett. **37A**, 251 (1971).

15. K. Hamada, M. Wakata, N. Sugii et al., Phys. Rev. B **48**, 6892 (1993).

16. I. R. Shein and A. L. Ivanovskii, Fiz. Tverd. Tela **45**, 1363 (2003).

17. A. Leithe-Jasper, A. Sato, T. Tanaka et al., Z. Kristallographie — New Crystal Structures **217**, 319 (2002).

18. I. R. Shein, N. I. Medvedeva, and A. L. Ivanovskii, Fiz. Tverd. Tela **45**, 1541 (2003).

19. M. Paranthaman, C. Cantoni, H. Y. Zhai et al., Appl. Phys. Lett. **78**, 3669 (2001).

20. V. A. Gasparov and A. P. Oganesyan, Physica C **178**, 445 (1991).

21. A. Gauzzi, J. Le Cochec, G. Lamura et al., Rev. Sci. Instr. **71**, 2147 (2000).

22. V. A. Gasparov, G. Tsydynzhapov, I. E. Batov, and Qi Li, E-print archives, cond-mat/0411220; (submitted to J. Low Temp. Phys.); V. A. Gasparov, I. Batov, Qi Li, and C. Kwon, Physica B **284–288**, 1021 (2000); Czech. J. Phys. **46** (Suppl. S3), 1401 (1996); Proc. SPIE **2697**, 391 (1996); Phys. Low-Dim. Struct. **6**, № 12, 36 (1995).

23. G. Lamura, E. Di Gennaro, M. Salluzzo et al., Phys. Rev. B **65**, 020506 (2002).

24. V. A. Gasparov, M. R. Mkrtchyan, M. A. Obolensky, and A. V. Bondarenko, Physica C **231**, 197 (1994).

25. V. A. Gasparov, M. P. Kulakov, N. S. Sidorov et al., Pis'ma v Zh. Eksp. Teor. Fiz. **80**, 376 (2004).

26. J. M. Ziman, *Electrons and Phonons, Theory of Transport Phenomena in Solids*, Oxford Univ. Press, Oxford (1960).

27. M. Putti, E. G. d'Agliano, D. Marré et al., Eur. Phys. J. B **25**, 439 (2002).

28. A. V. Sologubenko, J. Jun, S. M. Kazakov et al., Phys. Rev. B **66**, 014504 (2002).

29. N. V. Vol'kenshtein, V. P. Dyakina, and V. E. Startsev, Phys. Stat. Sol. **57**, 9 (1973).

30. V. A. Gasparov and R. Huguenin, Adv. Phys. **42**, 393 (1993).

31. I. I. Mazin, O. K. Andersen, O. Jepsen et al., Phys. Rev. Lett. **89**, 107002 (2002).

32. J. Halbritter, Z. Phys. **243**, 201 (1971).

33. W. N. Hardy, D. A. Bonn, D. C. Morgan et al., Phys. Rev. Lett. **70**, 3999 (1993).

34. D. A. Bonn, S. Kamal, K. Zhang et al., Phys. Rev. B **50**, 4051 (1994).

35. N. Schopohl and O. V. Dolgov, Phys. Rev. Lett. **80**, 4761 (1998); **81**, 4025 (1998).

36. A. Carrington, F. Manzano, R. Prozorov et al., Phys. Rev. Lett. **86**, 1074 (2001).

37. F. Manzano, A. Carrington, N. E. Hussey et al., Phys. Rev. Lett. **88**, 047002 (2002).

38. Yu. A. Nefyodov, M. R. Trunin, A. F. Shevchun et al., Europhys. Lett. **58**, 422 (2002).

39. R. S. Gonnelli, D. Daghero, G. A. Ummarino et al., Phys. Rev. Lett. **89**, 247004 (2002).

40. A. Brinkman, A. A. Golubov, H. Rogalla et al., Phys. Rev. B **65**, 180517(R) (2001); A. A. Golubov, A. Brinkman, O. V. Dolgov et al., Phys. Rev. B **66**, 054524 (2002).

41. F. Bouquet, Y. Wang, R. A. Fisher et al., Europhys. Lett. **56**, 856 (2001).

42. E. Helfand and N. R. Werthamer, Phys. Rev. Lett. **13**, 686 (1964); Phys. Rev. **147**, 288 (1966).

43. L. Lyard, P. Samuely, P. Szabo et al., Phys. Rev. B **66**, 180502 (R) (2002).

44. A. V. Sologubenko, J. Jun, S. M. Kazakov et al., Phys. Rev. B **66**, 180505 (R) (2002).

45. V. A. Gasparov, S. N. Ermolov, S. S. Khasanov et al., Physica B **284–288**, 1119 (2000).